A Hybrid CFD/BEM method for the calculation of
aeroacoustic noise from a radial fan

Hakan Dogan[1], Chris Eisenmenger[2], Martin Ochmann[1], Stefan Frank[2]

[1] *Beuth Hochschule für Technik, 13353 Berlin, E-Mail:hdogan, ochmann@beuth-hochschule.de*
[2] *Hochschule für Technik und Wirtschaft, 12459 Berlin, E-Mail: c.eisenmenger, stefan.frank@htw-berlin.de*

Introduction

Radial fans are used in many important engineering applications. In terms of design, it is desired to increase the efficiency of the fan and to reduce the aeroacoustic noise [1, 2]. In this study, the aerodynamic and acoustic performance of a radial fan used in household laundry dryers is investigated. Preliminary design guidelines of the fan considered were that backward curved blades are used and a logarithmic spiral housing is constructed, in order to increase the efficiency.

The aerodynamic performance of such fans is tested using a benchmark industry norm, e.g. ISO 5801 [3], which is carried out at the Turbomachinery Laboratory at HTW Berlin. In this test, the rotational speed is kept constant, the volumetric flow rate is varied over a range and the pressure rise is measured between the inlet and outlet in order to determine the efficiency of the fan. A radial fan with a diameter of 200 mm and nine backward-curved blades is used.

The aeroacoustic measurements are performed using a test rig (the so-called In-Duct method) according to the industry norm ISO 5136 [4], also installed at HTW Berlin. The far-field noise levels are recorded inside a circular duct using three slit-tube microphones (see Fig. 1).

In terms of numerical simulations, we employ a hybrid approach here, e.g. using computational fluid dynamics (CFD) and computational aeroacoustics (CAA). In the CFD simulations, the near field pressure and velocity values are computed with ANSYS-CFX software [5]. The far field acoustic pressure is evaluated using the direct boundary element (BEM) and FEM formulations. In particular, the Shear Stress Turbulence (SST) – based Stress-Blended Eddy Simulation model is used in CFD computations. A virtual interface near the beginning section of the duct (i.e. at y=0.3 m) is used for the data exchange (see Fig. 2). The acoustic pressure at the locations of the slit-tube microphones in the far-field is computed using BEM in this work. The comparison of the numerical results with the experimental values are shown.

Integral equation methods have been widely applied in computational aeroacoustics. Lyrintzis [6] presented a detailed review explaining the well-known Lighthill's analogy, Kirchhoff formulation and the Ffowcs-Williams Hawkings equation, and further improvements based on those formulations. In Ref. [7], the pressure-based integral equation method was applied to low Mach number duct acoustics. Sorguven and co-workers [8] used a hybrid large eddy simulation (LES) and boundary element method

(BEM) for the simulation of low Mach number aeroacoustics of a fan. Similarly, Piscoya et al. [9] used a LES-BEM approach for combustion noise. Piscoya and Ochmann [10] presented a dual reciprocity boundary element method (DRBEM) for convective wave propagation with non-uniform flow field. In Ref. [11], the local boundary integral equation (LBIE) method was implemented for the convective wave propagation with uniform flow for Mach number values of up to 0.5. The formulation employed in the present paper is similar to that used in Refs. [7, 9, 10].

Experiment test rig

As mentioned above, the acoustic noise is recorded using the experimental technique according to the industrial norm ISO 5136. The measurements were done with a duration of 35 seconds at each of the three microphones and were repeated 10 times. The recorded signals were post-processed with Samurai software from Sinus Acoustics. The Fourier transform of the signals were taken and averaged over all samples and microphones. Moreover, corrections due to the flow velocity and the shield protection of the microphones were done according to the formulas in Ref. [4].
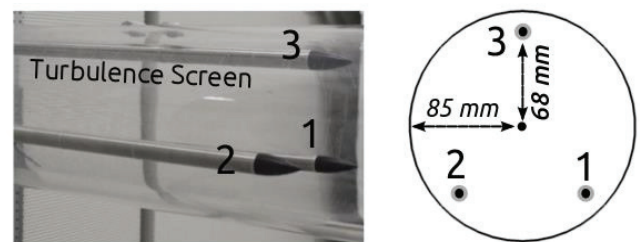

Figure 1: The high precision slit-tube microphones located inside the circular duct for the far field noise measurements. After Ref. [1].

Computational Fluid Dynamics

Several computational fluid dynamics simulations, such as the Detached Eddy Simulation (DES), Stress Blended Eddy Simulation (SBES) and the Scale Adaptive Simulation (SAS), have been performed in order to investigate the aerodynamic characteristic of the fan. The CFD mesh consisted of approximately 30-35 million nodes with mainly tetrahedral elements. Moreover, 15-20 prism layers were created near the solid walls in order to resolve the boundary layers.
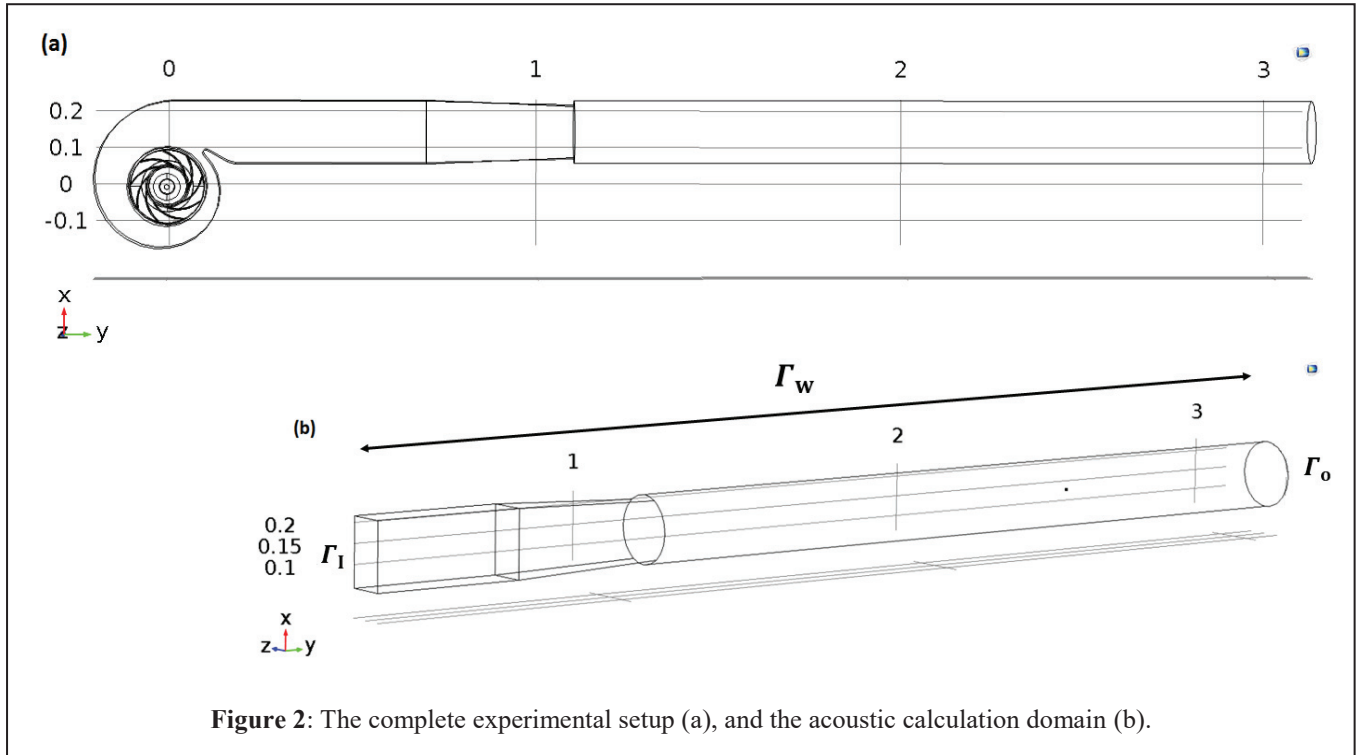
Figure 2: The complete experimental setup (a), and the acoustic calculation domain (b).

One of the primary aims of the CFD simulations is to calculate the static efficiency (η_{st}) of the fan, which is given by

$$\eta_{st} = \frac{\dot{V}\,\Delta p}{M\,2\pi n}, \tag{1}$$

where $\dot{V}$ is the volumetric flow rate, Δp is the pressure rise, n is the rotational speed and M is the total torque acting on the rotor.

The simulations were run for 8 revolutions of the rotor, where a converged steady solution was used as the initial condition. Hence, the last 4-6 revolutions of the simulations provided reliable time-dependent data. In Fig. 3, the hydrodynamic pressure fluctuations at a monitor point near the volute tongue during a simulation is shown.
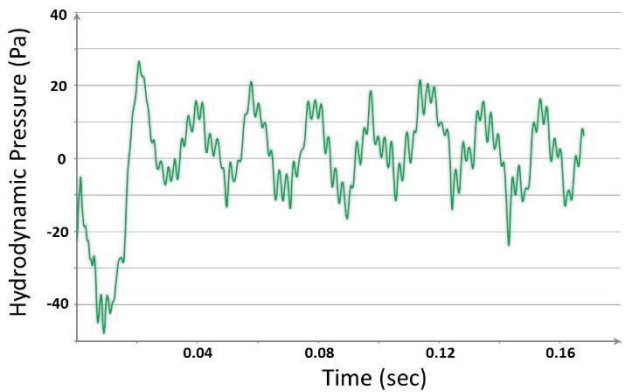

Figure 3: Hydrodynamic pressure fluctuations at a point in the flow domain near the volute tongue.

Acoustic Calculations

As mentioned in the Introduction, we use a virtual interface approach here, e.g. Kirchhoff surface, and employ a hybrid CFD/CAA simulation where the acoustic computation domain is set as the longitudinal duct from y=0.3m (inlet) to y=3.1m (outlet) as in Fig. 2b.

Let us denote the boundary enclosing the acoustic domain in Fig. 2b as $\Gamma = \Gamma_I \cup \Gamma_w \cup \Gamma_o$, where Γ_I is the permeable Kirchhoff surface (the inlet), Γ_o is the circular outlet of the duct, and Γ_w is the rigid side walls between the inlet and outlet. The acoustic pressure $p(x_i)$ at an internal point x_i within the domain can be obtained using the Helmholtz integral equation [9, 10]:

$$p(x_i) = \int_\Gamma G\frac{\partial p}{\partial n} - p\frac{\partial G}{\partial n}\,d\Gamma, \tag{2}$$

where the Green's function G is given by

$$G = \frac{e^{-ikr}}{4\pi r}. \tag{3}$$

In Eq. (3), r is the distance between the collocation point x_i and the integration points on the surface Γ, and k is the wavenumber.

In order to complete the above defined problem, the boundary conditions should be prescribed. At the permeable interface Γ_I, the acoustic pressure is prescribed by taking the Fourier transform of the time-domain pressure values (p_t) obtained in the CFD simulations:

$$p(\boldsymbol{x}, \omega) = \int_{-\infty}^{\infty} p_t(\boldsymbol{x})\, e^{-i\omega t}\, dt, \quad \boldsymbol{x} \in \Gamma_\mathrm{I}. \qquad (4)$$

On the rigid side walls, the particle velocity is zero. Therefore, the hard-wall condition is employed, i.e.

$$\frac{\partial p(\boldsymbol{x})}{\partial n} = 0 \qquad \boldsymbol{x} \in \Gamma_\mathrm{w}. \qquad (5)$$

At the outlet, the plane-wave impedance condition is prescribed:

$$Z(\boldsymbol{x}) = \rho\, c \qquad \boldsymbol{x} \in \Gamma_\mathrm{o}, \qquad (6)$$

where ρ is the density of the air and c is the speed of sound.

The set of equations (2), (4) -(6) is solved using the in-house developed direct boundary element method, which is based on discretising the integral terms in Eq. (2). For the numerical discretization, constant boundary elements with an edge length of maximum 0.010 m are used.

Results

The pressure fluctuations in the CFD simulations are computed on a grid which is considerably finer than the acoustic grid. Therefore, posterior to the Fourier transform applied in Eq. (4), we interpolate the frequency domain pressure values at the inlet Γ_I onto the acoustic grid. For the data interpolation, the radial basis functions (RBFs) are used. In the RBF approximation, the nearest neighbouring nodes (e.g. 20 nodes) in the fine grid are determined for each node in the coarse grid. A weight function based on the distances (R) between the nodes is used as the interpolation kernel. For instance, the thin plate spline function $R^2 \log(R)$ can be used for accurate interpolations on 2D surfaces. Further details of RBF can be found in [12].

Note that when the average acoustic pressure at the inlet surface is prescribed and the changes to the cross-sectional area of the duct are negligible as in the current problem, the acoustic pressure in the far-field inside the duct can be obtained analytically below the cut-off frequency by plane-wave propagation formulation, i.e.

$$p_{\mathrm{ac\_m}} = p_{\mathrm{avg}}\, e^{-ik(y_\mathrm{m}-y_\mathrm{I})}, \qquad (7)$$

where p_{avg} is the average frequency domain pressure value at the permeable surface at each value of wavenumber, y_I is the y-coordinate of the permeable surface, y_m is the y-coordinate of the microphones, and $p_{\mathrm{ac\_m}}$ is the acoustic pressure value at the microphone locations.

In Fig. 4, the numerical values for the acoustic pressure obtained using the BEM at the three microphone locations are shown, and compared to the analytical solution given by Eq. (7). It can be noticed that the numerical results agree very well with the analytical formula up to the frequency value of 1200 Hz. The location of the microphone within the circular cross-section of the duct creates differences in the numerical results above that frequency. In fact, for the

considered experimental test rig and the geometry, the circular outlet duct has a cut-off frequency of approximately 1170 Hz [4].
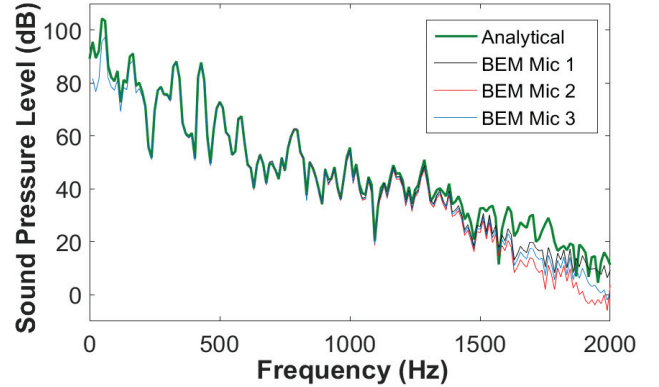
Figure 4: Comparison of the analytical solution for plane-wave propagation inside the duct with the numerically obtained values at the three microphone positions.

In Fig. 5, the numerical results for the acoustic pressure is compared with the experimental data. As mentioned above, the experimental data is averaged over the three microphone recordings, as well as the repeated ten measurement sets. The blade passing frequency (BPF) of the problem is 429 Hz. The numerical results at the BPF indicate a sound pressure level (SPL) of ~86 dB, which lies within 3-4dB difference with the experimental value. The SPLs between the numerical and the experimental results agree considerably within the frequency range 500-1100 Hz, whereas above this range the numerical results underestimate the pressure spectrum.
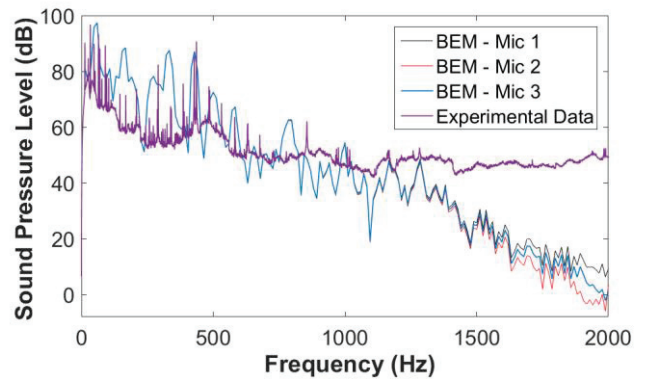
Figure 5: Numerically obtained values sound pressure levels at three microphone positions vs. the experimental result.

The results shown here have included only the SPLs. In order to present more accurate comparisons, the power spectral density results will be calculated as a future work. Furthermore, in order to eliminate the differences due to the frequency resolution and the total time duration of the experimental data and the numerical simulation, additional normalization operations are required as described in Ref. [1].

Conclusions

In this work, the aerodynamic and the aeroacoustic characteristics of a radial fan is investigated. A backward curved fan with nine blades and a diameter of 200 mm has been designed and prototyped. For the near field simulations, various CFD computations, e.g. SAS and SBES formulations on different meshes (for example, SAS and SBES are the hybrid turbulence models), have been performed in order to determine to most suited numerical method. The computational aeroacoustics approach is based on determining an acoustic domain to simulate the propagation to the far field where the Helmholtz integral equation holds. A permeable interface located towards the beginning of the duct has been used for the data exchange between CFD and CAA calculations.

The comparisons between the experimental data and the numerical simulations presented in the current article indicate preliminary good agreement. Further refinements will be performed in terms of both investigations in order to improve the design parameters such as efficiency and radiated sound power levels.

Acknowledgements

GEFÖRDERT VOM

Bundesministerium
für Bildung
und Forschung

FORSCHUNG AN
FACHHOCHSCHULEN

References

[1] Darvish, M.; Frank, S.; Paschereit, C. O.: Numerical and experimental study on the tonal noise generation of a radial fan. Journal of Turbomachinery 137(101005) (2015), 1-9

[2] C. Eisenmenger, S. Frank, H. Dogan, M. Ochmann: High Efficiency Low Noise Heatpump Dryer (HELNoise). Proc. 43. Jahrestagung für Akustik-DAGA (2017) 1491-1494

[3] Industrial Organization for Standardization, ISO 5801: Industrial Fans – Performance testing using standardized airways (2011) London

[4] Industrial Organization for Standardization, ISO 5136: Acoustics – Determination of sound power radiated into a duct by fans and other air-moving devices (2003) London

[5] ANSYS – CFX, URL: http://www.ansys.com/Products/Fluids/ANSYS-CFX

[6] Lyrintzis, A. S.: Surface integral methods in computational aeroacoustics – From the (CFD) near field to the (Acoustic) far field. International Journal of Aeroacoustics 2(2) (2003), 95-128

[7] N. Papaxanthos, E. Perrey-Debain, S. Bennouna, B. Ouedraogo, S. Moreau, J. M. Ville: Pressure-based integral formulations of Lighthill-Curle's analogy for internal aeroacoustics at low Mach numbers. Journal of Sound and Vibration 393 (2017) 176-186

[8] Sorguven, E.; Dogan, Y.; Bayraktar, F.; Sanliturk, K. Y.: Noise prediction via large eddy simulation: Application to radial fans. Noise Control Engineering Journal 57(3) (2009), 169-178

[9] Piscoya, R.; Brick, H.; Ochmann, M.; Költzsch, P.: Equivalent source method and boundary element method for calculating combustion noise. Acta Acustica United with Acustica 94 (2008), 514-527

[10] Piscoya, R.; Ochmann, M.: Acoustical boundary elements: Theory and virtual experiments. Archives of Acoustics 39(4) (2014), 453-465

[11] H. Dogan, C. Eisenmenger, M. Ochmann, S. Frank: A LBIE-RBF solution to the convected wave equation for flow acoustics. Engineering Analysis with Boundary Elements (2018) In Press, DOI: doi.org/10.1016/j.enganabound.2017.11.016

[12] Dogan, H.; Popov, V.; Ooi, E. H.: Dispersion analysis of the meshless local boundary integral equation and radial basis integral equation methods for the Helmholtz equation. Engineering Analysis with Boundary Elements 50 (2016), 360-371